Int. J. Solids Structures Vol. 17, pp. 127–143
Pergamon Press Ltd., 1981. Printed in Great Britain

NUMERICAL ANALYSIS OF PLANAR, TIME-DEPENDENT INELASTIC DEFORMATION OF PLATES WITH CRACKS BY THE BOUNDARY ELEMENT METHOD

MAHESH MORJARIA and SUBRATA MUKHERJEE
Department of Theoretical and Applied Mechanics, Cornell University, Ithaca, NY 14853, U.S.A.

(*Received* 2 *February* 1980; *in revised form* 22 *April* 1980)

Abstract—A boundary element formulation using augmented kernels, for planar time-dependent inelastic deformation problems for bodies with cutouts, has been presented in a companion paper[1]. The primary advantage of this formulation is that the effect of the cutout is incorporated in the kernels and the cutout boundary need not be modelled in a numerical solution procedure. In this paper, the specific kernels for plates with elliptic cutouts are first derived. These kernels are then used to obtain numerical solutions for time-dependent stress fields near stationary crack tips in finite plates. A crack is modelled as a very narrow ellipse and both remote tensile (mode one) and remote shear (mode two) loadings are considered. The deformation of the plate material is assumed to be described either by the equations of power law creep or the combined creep-plasticity constitutive model of Hart.

INTRODUCTION

A boundary element formulation for planar time-dependent inelastic deformation of plates with cutouts has been presented in a companion paper[1]. In that formulation a stress function description is used and a nonhomogeneous biharmonic equation for the rate of the stress function is obtained. The nonhomogeneous term is due to the presence of nonelastic strains. This differential equation is transformed into an integral equation for certain concentrations on the boundary, using, as kernels, augmented versions of the usual singular fundamental solutions of the biharmonic equation in an infinite plane. These augmented kernels guarantee that the cutout boundary remains traction free for all time. Thus, the effect of the cutout on the stress field is incorporated into the kernels and discrete modelling of the cutout boundary is not necessary. This approach leads to an accurate determination of stresses, especially in the near field of the cutout.

The problem of inelastic deformation of plates with cracks is of considerable importance. Riedel and Rice[2, 3], for example, have recently studied the stress fields in cracked bodies undergoing elastic–viscoplastic deformation. In this paper, a crack is modelled as a very thin ellipse. It is well known that the presence of thin elliptical cutouts in plates causes very large concentrations of stresses on and near certain points on the cutout boundary and accurate determination of these stresses is one of the primary concerns in fracture mechanics. In problems of inelastic fracture mechanics, where nonelastic strain rates are typically proportional to high powers of stress, these regions of strain rate concentration provide nearly all the inelastic contribution to stress rates. Thus, it is imperative that stresses in the near field of the cracks be obtained very accurately if the redistribution of stresses with time is to be determined with sufficient accuracy.

An earlier direct boundary element formulation presented by the authors[4] uses Kelvin kernels for concentrated forces in an infinite plane. That formulation requires discrete modelling of the cutout boundary and a very large number of boundary elements are usually needed near crack tips in order to obtain the stresses accurately in these regions. This situation may cause numerical problems. In the present approach, as stated earlier, the crack boundary need not be modelled in the numerical calculations and an accurate and efficient determination of stresses near the crack is possible.

In this paper, a restatement of the integral equation formulation[1] is followed by the derivation of the modified kernels for plates with elliptical cutouts. A numerical implementation of the integral equations using a piecewise linear description of the unknown concentrations on the physical boundary of the body is given next. Finally, numerical results for mode I and mode II cracks in finite square plates are presented. The time-dependent redistribution of stresses in the near field of the cracks is studied in some detail. The constitutive models used in the

numerical calculations are power law creep[5] and the combined creep-plasticity constitutive model of Hart[6, 7]. Numerical results using other constitutive models having the mathematical structure of these equations, can be easily obtained if desired.

BOUNDARY ELEMENT FORMULATION

Governing differential equation

The governing biharmonic equation for the rate of the stress function $\dot{\Phi}$, for inelastic deformation of a planar body, can be obtained as[1]

$$\nabla^4\dot{\Phi} = C^{(n)} \tag{1}$$

where, for plane strain

$$C^{(n)} = -\frac{E}{1-\nu^2}\left[\frac{\partial^2\dot{\epsilon}^n_{11}}{\partial x_2{}^2} + \frac{\partial^2\dot{\epsilon}^n_{22}}{\partial x_1{}^2} - \frac{2\partial^2\dot{\epsilon}^n_{12}}{\partial x_1\partial x_2} + \nu\nabla^2(\dot{\epsilon}^n_{11} + \dot{\epsilon}^n_{22})\right]$$

with E the Young's modulus, ν the Poisson's ratio, $\dot{\epsilon}^n_{ij}$ the nonelastic strain rates, ∇ the gradient operator and x_i a set of orthogonal cartesian axes with x_1 and x_2 in the plane of the body.

The equation has the same form for plane stress with ν set equal to zero.

Integral equations

An integral formulation for the stress rates $\dot{\sigma}_{ij}(i, j = 1, 2)$ has the form (see Fig. 4 of [1])

$$8\pi\dot{\sigma}_{ij}(p) = \oint_{\partial B_2} H^{(1)}_{ij}(p, Q)C_1(Q)\,\mathrm{d}c_Q + \oint_{\partial B_2} H^{(2)}_{ij}(p, Q)C_2(Q)\,\mathrm{d}c_Q$$
$$+\oint_{\partial B_2} H^{(1)}_{ij}(p, Q)D^{(n)}_k(Q)n_k(Q)\,\mathrm{d}c_Q - \int_B H^{(1)}_{ij,k_0}(p, q)D^{(n)}_{k_0}(q)\,\mathrm{d}A_q. \tag{2}$$

Here p (or P) is a source point and q (and Q) is a field point, with capital letters denoting points on the boundary of the body ∂B_2 and lower case letters denoting points inside the body B. The functions C_1 and C_2 are layers of boundary concentrations to be determined from the boundary traction rates. The vector function $\mathbf{D}^{(n)}$, for plane strain, is

$$D_1{}^{(n)} = \frac{E}{1-\nu^2}\left[-\frac{\partial\dot{\epsilon}^n_{22}}{\partial x_1} + \frac{\partial\dot{\epsilon}^n_{12}}{\partial x_2} - \nu\frac{\partial}{\partial x_1}(\dot{\epsilon}^n_{11} + \dot{\epsilon}^n_{22})\right]$$
$$D_2{}^{(n)} = \frac{E}{1-\nu^2}\left[\frac{\partial\dot{\epsilon}^n_{12}}{\partial x_1} - \frac{\partial\dot{\epsilon}^n_{11}}{\partial x_2} - \nu\frac{\partial}{\partial x_2}(\dot{\epsilon}^n_{11} + \dot{\epsilon}^n_{22})\right]$$

and, for, plane stress, $D_1{}^{(n)}$ and $D_2{}^{(n)}$ have the same form as above with ν set equal to zero. The outward normal on ∂B_2 has components n_k, k_0 denotes a field point, and the kernels $H^{(k)}_{ij}$ are derived from the functions $\phi_k(z, z_0)$ and $\psi_k(z, z_0)$ $(k = 1, 2)$ according to the formulae

$$H^{(k)}_{11}(z, z_0) = \mathrm{Re}\,[2\phi'_k(z, z_0) - \bar{z}\phi''_k(z, z_0) - \psi'_k(z, z_0)]$$
$$H^{(k)}_{22}(z, z_0) = \mathrm{Re}\,[2\phi'_k(z, z_0) + \bar{z}\phi''_k(z, z_0) + \psi'_k(z, z_0)$$
$$H^{(k)}_{12}(z, z_0) = \mathrm{Im}\,[\bar{z}\phi''_k(z, z_0) + \psi'_k(z, z_0)]$$

where a prime denotes differentiation with respect to the complex variable z, a superscribed bar denotes a complex conjugate and Re and Im denote, respectively, the real and imaginary parts of the quantities within brackets.

The traction rates $\dot{\tau}_i$ at a point P on the boundary where it is locally smooth are

$$8\pi\dot{\tau}_i(P) = \oint_{\partial B_2} H_{ij}^{(1)}(P, Q)n_j(P)C_1(Q)\,dc_Q + \oint_{\partial B_2} H_{ij}^{(2)}(P, Q)n_j(P)C_2(Q)\,dc_Q$$
$$+ \oint_{\partial B_2} H_{ij}^{(1)}(P, Q)D_k^{(n)}(Q)n_j(P)n_k(Q)\,dc_Q$$
$$- \int_B H_{ij,k_0}^{(1)}(P, q)D_{k_0}^{(n)}(q)n_j(P)\,dA_q \quad (i, j, k = 1, 2) \tag{3}$$

The formulae for normal and shearing stress rates at a point P on the boundary can be derived directly from eqn (2) but the formula for the tangential stress rate $\dot{\sigma}_{cc}$ has a residue of $4\pi C_2$ as p approaches P on the boundary where it is locally smooth, i.e. if

$$8\pi\dot{\sigma}_{cc}(p^*) = h(p^*)$$

then

$$8\pi\dot{\sigma}_{cc}(P^*) = h(P^*) + 4\pi C_2(P^*)$$

where p^* is infinitesimally close to P^*.

The functions ϕ_k and ψ_k $(k = 1, 2)$ from which the kernels $H_{ij}^{(k)}$ of eqn (2) are obtained, are derived by using the methods of Muskhelishvili[8]. Following the methods outlined in [1], the appropriate mapping function in this case is (see Fig. 1)

$$z = \omega(\xi) = \frac{1}{\xi} + m\xi \tag{4}$$

where $m = (a - b)/(a + b)$ (with $(a + b)/2 = 1$), in terms of the semi major and minor axes of the ellipse. Thus, $m = 0$ represents a circular cutout and $m = 1$ a line crack. This function maps the region on and outside the ellipse in the z plane to the region on and inside an unit circle in the ξ plane as shown in Fig. 1. The functions ϕ_i and ψ_i, within additive functions of z_0, are

$$\phi_1(z, z_0) = (z - z_0)\ln(z - z_0) - m\xi - m\xi\ln m - (m\xi - z_0)[\ln(\xi - r_0) + \ln(\xi - t_0)]$$
$$-\frac{1}{\xi}[\ln(1 - \xi/r_0) + \ln(1 - \xi/t_0)] \tag{5}$$

$$\psi_1(z, z_0) = -\bar{z}_0\ln(z - z_0) - \xi - \xi\ln m - (\xi - \bar{z}_0)[\ln(\xi - r_0) + \ln(\xi - t_0)]$$
$$-\frac{m}{\xi}[\ln(1 - \xi/r_0) + \ln(1 - \xi/t_0)] + \frac{\xi^2 + m}{1 - m\xi^2}\left[-m\xi[\ln m + 1 + \ln(\xi - r_0) + \ln(\xi - t_0)]\right.$$
$$\left. - \xi(m\xi - z_0)\left[\frac{1}{\xi - r_0} + \frac{1}{\xi - t_0}\right] + \frac{1}{\xi}[\ln(1 - \xi/r_0) + \ln(1 - \xi/t_0)] - \frac{1}{\xi - r_0} - \frac{1}{\xi - t_0}\right] \tag{6}$$

$$\phi_2 = \frac{\partial\phi_1}{\partial n_0}, \qquad \psi_2 = \frac{\partial\psi_1}{\partial n_0} \tag{7, 8}$$

where

$$\xi = \frac{z \pm \sqrt{(z^2 - 4m)}}{2m}$$

$$r_{0,i} = \frac{z_0 \pm \sqrt{(z_0^2 - 4m)}}{2m} \text{ are the roots of } m\xi^2 - z_0\xi + 1 = 0$$

$$t_{0,i} = \frac{\bar{z}_0 \pm \sqrt{(\bar{z}_0^2 - 4m)}}{2} \text{ are the roots of } \xi^2 - \bar{z}_0\xi + m = 0$$

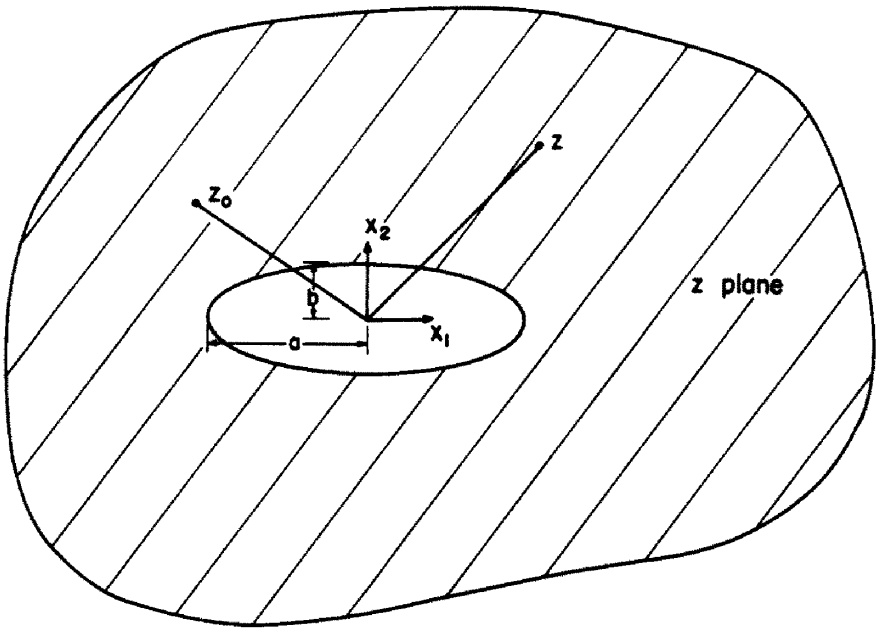

Fig. 1(a). Plate with elliptical cutout, z plane.

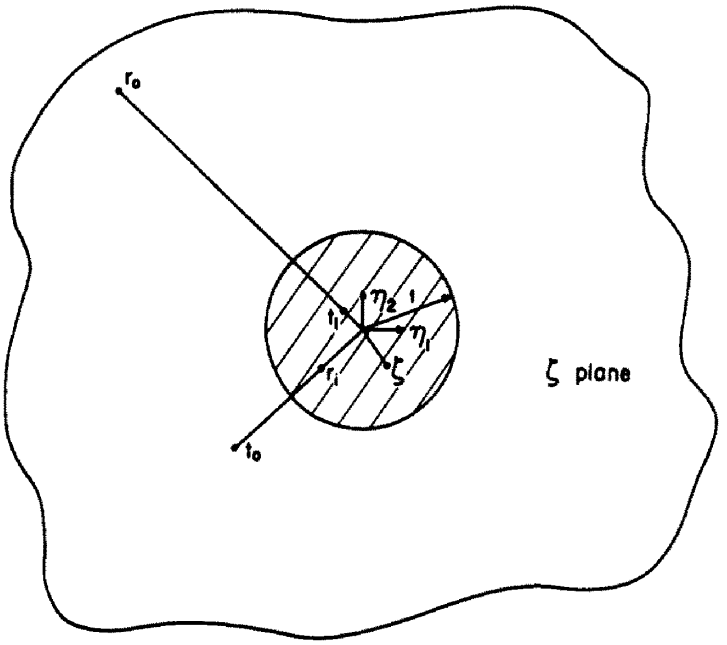

Fig. 1(b). Plate with elliptical cutout, ξ plane.

with

$$|\xi| \leq 1, \quad |r_0| \geq 1, \quad |t_0| \geq 1.$$

NUMERICAL IMPLEMENTATION

Discretization of equations

The outer boundary of the planar body with a cutout, ∂B_2, (see Fig. 4 of [1]) is divided into N_s straight boundary elements using N_b ($N_b = N_s$) boundary nodes and the interior of the body,

B, is divided into n_i triangular internal elements. A discretized version of eqn (3) is

$$8\pi\dot{\tau}_i(P_M) = \sum_{N_s}\int_{\Delta c_j} H_{ij}^{(1)}(P_M, Q)n_j(P_M)C_1(Q)\,\mathrm{d}c_Q + \sum_{N_s}\int_{\Delta c_j} H_{ij}^{(2)}(P_M, Q)n_j(P_M)C_2(Q)\,\mathrm{d}c_Q + \sum_{N_s}\int_{\Delta c_j} H_{ij}^{(1)}(P_M, Q)D_k^{(n)}(Q)n_j(P_M)n_k(Q)\,\mathrm{d}c_Q - \sum_{n_i}\int_{\Delta A_j} H_{ij,k_0}^{(1)}(P_M, q)D_{k_0}^{(n)}(q)n_j(P_M)\,\mathrm{d}A_q \quad (i, j, k = 1, 2,\ M = 1, 2, \ldots N_s) \tag{9}$$

where $\tau_i(P_M)$ are the traction components at the point P which coincides with node M and Δc_j and ΔA_j are boundary and internal elements respectively. The concentrations C_1 and C_2 are assumed to vary linearly over each boundary element with (generally) their values assigned at the nodes which lie at the intersections of these elements. Possible discontinuities in C_1 and C_2 (for example, across corners) are taken care of by placing a zero length element between two boundary nodes and assigning different values of concentrations at these nodes. Also, for boundary elements adjacent to a corner, the source points are placed slightly away from the corner itself, in order to avoid taking a limit at a point on the boundary where it is not locally smooth.

The nonelastic strain rates $\dot{\epsilon}_{jk}^n$ are interpolated linearly over each triangular internal element. Hence, the components of $\mathbf{D}^{(n)}$ are uniform within each element. Integrals of $H_{ij}^{(k)}$ and $cH_{ij}^{(k)}$ on boundary elements are evaluated by Gaussian integration except analytically for singular terms. Integrals on internal elements are always evaluated by Gaussian integration. The integrands in this case are never singular since the Gauss points never coincide with the source points which lie on the vertices (nodes) of the triangles.

Substitution of the linear functional forms of C_1 and C_2 into eqn (9) leads to an algebraic system of the type

$$\{\dot{\tau}\} = [A]\{x\} + \{d\}. \tag{10}$$

The coefficients of the matrix $[A]$ contain boundary integrals of the kernels. The traction rates are prescribed, the vector $\{d\}$ contains integrals of the kernels and the nonelastic strain rates and the vector $\{x\}$ contains the unknown values of the concentrations at the boundary nodes.

Equation (2) for stress rates at an internal point p is discretized in a similar fashion.

Solution strategy

The class of constitutive models for material behavior, admissible in this BEM formulation, has the following mathematical structure (see [1])

$$\dot{\epsilon}_{ij} = \dot{\epsilon}_{ij}^e + \dot{\epsilon}_{ij}^n,\ \dot{\epsilon}_{ij}^n = h_{ij}(\sigma_{ij}, q_{ij}^{(k)}) \tag{11, 12}$$

$$\dot{q}_{ij}^{(k)} = g_{ij}(\sigma_{ij}, q_{ij}^{(k)}),\ \dot{\epsilon}_{kk}^n = 0. \tag{13, 14}$$

Here $\dot{\epsilon}_{ij}^e$ and $\dot{\epsilon}_{ij}^n$ are the elastic and nonelastic strain rates and $q_{ij}^{(k)}$ are state variables. (As stated earlier in [1], the thermal strain rates are set to zero for the sake of simplicity and only uniform temperature problems are considered here.) It is important to note that the rates of the nonelastic strain and state variables, at any time, depend only on the current values of the stress and state variables.

The initial values of the state variables are prescribed and the initial stress field is obtained by solving the corresponding elastic problem. The initial rates of the nonelastic strain rates and state variables are obtained from the constitutive eqns (12)–(14). The vector $\mathbf{d}$ in eqn (10) is

calculated next, and this, together with the prescribed rates of boundary tractions, are used to calculate the initial values of the boundary concentrations C_1 and C_2. These concentrations are now used in a discretized version of eqn (2) to calculate the initial stress rates throughout the body. These rates are used to find the values of the variables after a small time interval Δt and so on, and in this way the time histories of the relevant variables are obtained.

Time-integration is carried out by a step-wise procedure with automatic time-step control. An Euler-type strategy[9] which is simple, yet very efficient, is used to obtain the numerical results presented in the next section. A brief summary of the method in terms of a single differential equation

$$\frac{dy}{dt} = F(y, t) \tag{15}$$

is presented below. The value of $y(t+\Delta t)$ in terms of $y(t)$ is

$$y(t+\Delta t) = y(t) + F(y, t)\Delta t \tag{16}$$

and the error at this step used for automatic time-step control is defined as

$$e = \Delta t|\nabla F|/|y(t)| \tag{17}$$

where $\nabla F = F(y, t) - F(y, t - \Delta t_{\text{previous}})$, is the first backward difference of F. Two error parameters $e_{\max}$ and $e_{\min}$ are initially prescribed. The algorithm proceeds as follows:

$$e_{\max} < e\text{: replace } \Delta t \text{ by } \Delta t/2\text{; recompute } e$$

$$e \le e_{\max}\text{: accept } \Delta t\text{; calculate } y(t+\Delta t).$$

The time step for the next step, Δt_{next}, is decided according as

$$e_{\min} < e \le e_{\max}\text{: } \Delta t_{\text{next}} = \Delta t$$

$$e \le e_{\min}\text{: } \Delta t_{\text{next}} = 2\Delta t.$$

The problem at hand, of course, involves systems of such equations for the rates of variables at the boundary and internal nodes. In this case, the error e_i for the ith variable is defined as an L^1 norm of the type

$$e_i = \frac{\Delta t \Sigma |\nabla F_k|}{\Sigma |y_k(t)|} \tag{18}$$

$$e_i = \frac{\Delta t \Sigma |\nabla F_k|}{\Sigma |y_k(t)|} \tag{18}$$

where the summation extends over the values of the ith variable over all nodes; and then

$$e = \max |e_i|. \tag{19}$$

The algorithm then proceeds as described above.

NUMERICAL RESULTS AND DISCUSSION

Power law creep constitutive model

The equations for power law creep are[5]

$$\dot{\epsilon}^n = \dot{\epsilon}_c \left(\frac{\sigma}{\sigma_c}\right)^{m_0}, \quad \dot{\epsilon}^n_{ij} = \frac{3}{2}\frac{\dot{\epsilon}^n}{\sigma} s_{ij} \tag{20, 21}$$

where the stress and strain rate invariants are defined as

$$\sigma = \sqrt{[(3/2)s_{ij}s_{ij}]},\ \dot{\epsilon}^n = \sqrt{[(2/3)\dot{\epsilon}^n_{ij}\dot{\epsilon}^n_{ij}}$$

with s_{ij} the deviatoric part of the stress tensor σ_{ij}, $\dot{\epsilon}_c$ and σ_c reference strain rate and reference stress respectively and m_0 the index of the power law.

Hart's constitutive model

According to this model, the nonelastic strain rate is decomposed into two (time-dependent) components

$$\dot{\epsilon}^n_{ij} = \dot{\epsilon}^a_{ij} + \dot{\epsilon}^p_{ij} \tag{22}$$

where ϵ^a_{ij} is the anelastic strain, a stored strain which reflects the magnitude and direction of prior deformation history and ϵ^p_{ij} is the completely irrecoverable and path dependent permanent strain. The two state variables in the model are the anelastic strain and a scalar σ^*, called hardness, which is similar to an isotropic strain hardening parameter. The constitutive equations prescribe flow rules for the anelastic strain tensor and the permanent and nonelastic strain rates. Two auxillarytensors s^a_{ij} and s^f_{ij} are used and their sum equals s_{ij}. Certain scalar invariants of the relevant tensors are defined in the usual way (e.g. $\sigma^a = \sqrt{[(3/2)s^a_{ij}s^a_{ij}]}$ and these are related to each other through the uniaxial equations

$$\sigma^a = \mathcal{M}\epsilon^a,\ \dot{\epsilon}^n = \dot{\epsilon}_0(\sigma^f/\sigma_0)^M \tag{23, 24}$$

$$\dot{\epsilon}^p = \dot{\epsilon}^*(\ln(\sigma^*/\sigma^a))^{-1/\lambda} \tag{25}$$

$$\dot{\epsilon}^* = \dot{\epsilon}^*_{sT}(\sigma^*/\sigma^*_s)^{\bar{m}} \exp(Q/RT_B)\exp(-Q/RT) \tag{26}$$

$$\dot{\sigma}^* = \dot{\epsilon}^p\sigma^*\Gamma(\sigma^*, \sigma^a),\ \Gamma(\sigma^*, \sigma^a) = (\beta/\sigma^*)^\delta(\sigma^a/\sigma^*)^{\beta/\sigma^*} \tag{27, 28}$$

Equation (23) represents a linear anelastic element, (24) a nonlinear dashpot, (25) and (26) a "plastic" element and, finally, (27) and (28) describe strain hardening. The flow parameters are $\mathcal{M}$, M, $\bar{m}$, λ, $\dot{\epsilon}_0$ (at a reference stress level σ_0) and $\dot{\epsilon}^*_{sT}$ (at reference hardness level σ^*_s and reference temperature T_B); β and δ are strain hardening parameters, R is the gas constant and Q the activation energy for atomic self diffusion. The material parameters, many of which are temperature dependent, are obtained from load relaxation and constant strain rate tension experiments. They are given in Appendix A of the EPRI report by Kumar *et al.*[10].

The power law creep model is an example of a "traditional" creep theory and Hart's model is an example of a "newer" theory with state variables. This combined creep-plasticity model due to Hart has been carefully investigated recently and close correlation between theory and experiment has been obtained for several cases[10]. Both these models have a mathematical structure described by eqns (11)–(14). As stated earlier, other constitutive models having a similar mathematical structure can also be used in numerical examples for this BEM formulation.

Material parameters

The numerical examples, described in the next section, use material parameters for stainless at 400°C. The elastic constants at 400°C are

$$E = 0.244 \times 10^8 \text{ psi}\ \ \nu = 0.298.$$

The parameters for power law creep for 18 Cr 8 Ni stainless steel, from Ref.[11] are

$$\dot{\epsilon}_c = 0.277 \times 10^{-3}\ \text{s}^{-1}\ \ \sigma_c = 0.1806 \times 10^6 \text{ psi}$$

$$m_0 = 7.$$

The parameters for Hart's model for 304 stainless steel from Ref. [10], are

$$\lambda = 0.15 \quad M = 7.8 \quad \bar{m} = 5$$

$$\mathcal{M} = 0.132 \times 10^8 \text{ psi}$$

$$\dot{\epsilon}_0 = 1.0 \text{ at } \sigma_0 = 8631.9 \text{ psi}$$

$$\dot{\epsilon}^*_{sT} = 1.269 \times 10^{-24} \text{ s}^{-1} \text{ at } \sigma^*_s = 10{,}000 \text{ psi and}$$

$$T_B = 673°\text{K}$$

$$\beta = 0.179 \times 10^6 \text{ psi} \quad \delta = 1.33.$$

The initial values of state variables for an annealed specimen are

$$\sigma^*(\mathbf{x}, 0) = 17 \text{ ksi} \quad \epsilon^a_{ij}(\mathbf{x}, 0) = 0.$$

Numerical results for plane stress

Comparison with previous calculations. A square plate with an elliptical cutout of axis ratio 4 is loaded by an uniform remote stress of 4000 psi in the direction of the minor axis (the 2 direction). Quarter symmetry is used and 12 boundary nodes are distributed uniformly on the edges $x_1 = l$, $0 \le x_2 \le l$ and $x_2 = l$, $0 \le x_1 \le l$ of the plate. The internal element distribution for this problem is shown in Figs. 2(a) and (b). Due to the facts that the stresses are nearly uniform far from the ellipse and that $\mathbf{D}^{(n)}$ depends on strain rate gradients, only a portion of the plate is discretized into internal elements. It is assumed that all the nonelastic contribution to the stress rates in eqn (2) is obtained from this discretized area. This leads to a substantial saving in cost since fewer internal elements are necessary.

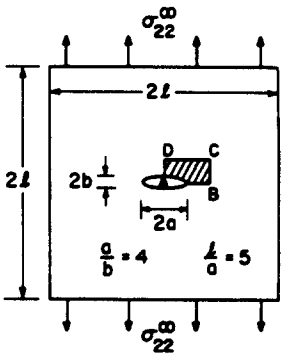

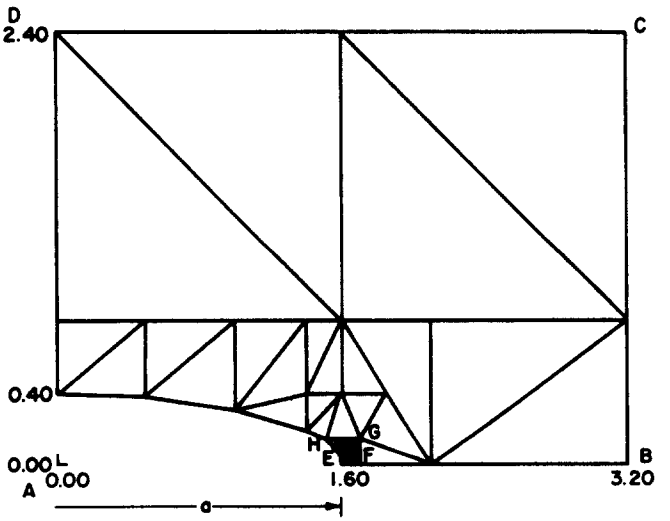

Fig. 2(a). Internal elements for plate with elliptical cutout of axis ratio 4:1 under uniaxial tension.

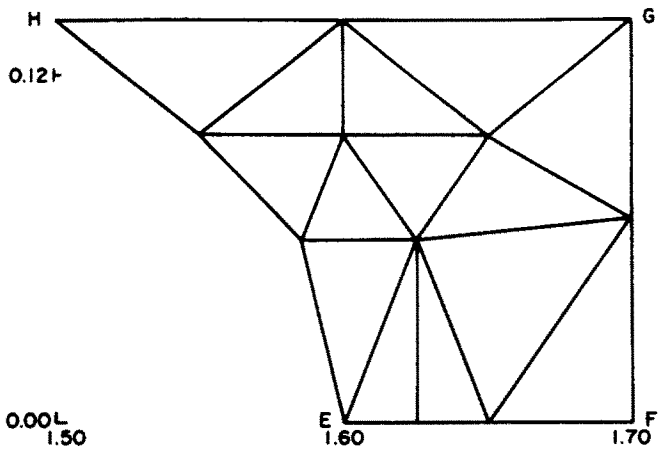

Fig. 2(b). Further details of Fig. 2(a).

The redistribution of stress concentration $\sigma_{22}/\sigma_{22}^{\infty}$ with time along the line $x_2 = 0$ is shown in Fig. 3. The results are compared with those from Ref. [4] where a direct formulation with Kelvin kernels was used. The results at zero time coincide within plotting accuracy and those at 100 hours agree quite well. The current results are obtained from a linear interpolation of the nonelastic strain rates over an internal element. They are expected to be more accurate than those from Ref. [4] where a spatially uniform description of these quantities over each internal element was used.

Mode one crack results. A crack is modelled as a thin ellipse with axis ratio 199 ($m = 0.99$). The plate with the crack is loaded by a remote stress in the x_2 direction increasing at a constant rate. The region very near the tip of the major axis of the ellipse is discretized into internal elements as shown on Figs. 4(a) and (b). Quarter symmetry is used and 12 boundary nodes are distributed uniformly along the edges of the plate in the first quadrant.

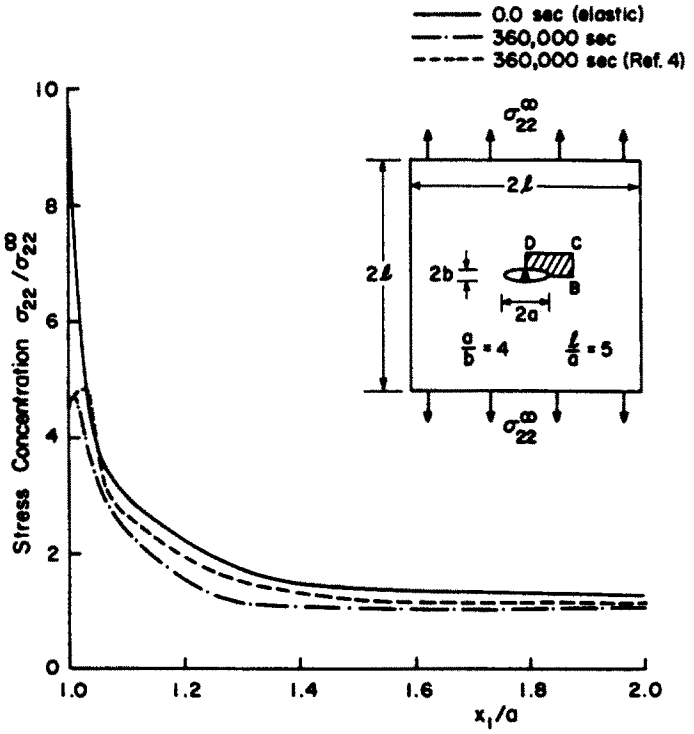

Fig. 3. Stress redistribution along the line $x_2 = 0$ in plate with elliptical cutout of axis ratio 4:1. Uniaxial tension $\sigma_{22}^{\infty} = 4$ ksi. Hart's model.

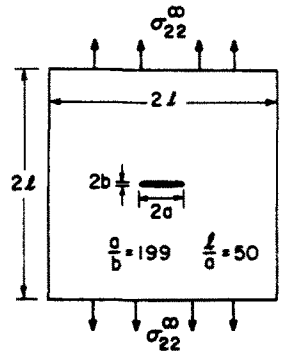

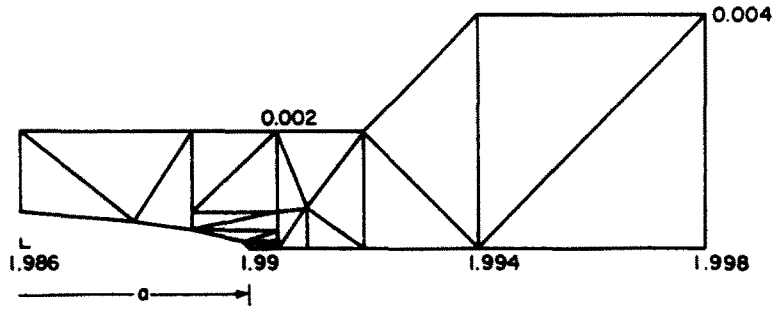

Fig. 4(a). Internal elements for cracked plate under uniaxial tension.

The decrease of stress concentration at the tip of the major axis of the ellipse as a function of the remote stress (i.e. $\dot{\sigma}_{22}^{\infty} \times$ time) is shown in Figs. 5 and 6 for power law creep and Hart's model respectively. The elastic stress concentration for an infinite plate in this case is 399. The decrease of stress concentration with time is due to flow of the material in the high stress region near the crack tip and consequent accomodation of stress. The constitutive models include rate dependence and stress relaxation is less at the higher loading rate since there is less time for plastic flow in this case. The time scales are different in the two figures because Hart's model, in this example, describes short time transient behavior, while the power law creep equations essentially model secondary creep.

The distribution of stresses in a small region near the crack tip, along the extension of the major axis of the ellipse, is shown in Figs. 7 (power law) and 8 (Hart's model). The stress plots in Fig. 8 show the stress state when the remote stress reaches 222 psi. The stress component σ_{11} is seen to increase from zero to a substantial stress concentration within a short distance from the crack tip, before dropping off. As mentioned before, there is more stress relaxation near the crack tip for the lower loading rate. The situation is reversed away from the crack tip in order to satisfy equilibrium. The growth of the viscoplastic region with time for this case, from Hart's constitutive model, is shown in Fig. 9. The boundaries are free-hand sketches obtained from a knowledge of internal elements that have entered the viscoplastic limit[10]. The viscoplastic limit

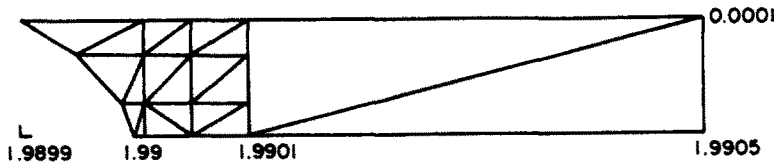

Fig. 4(b). Further details of Fig. 4(a).

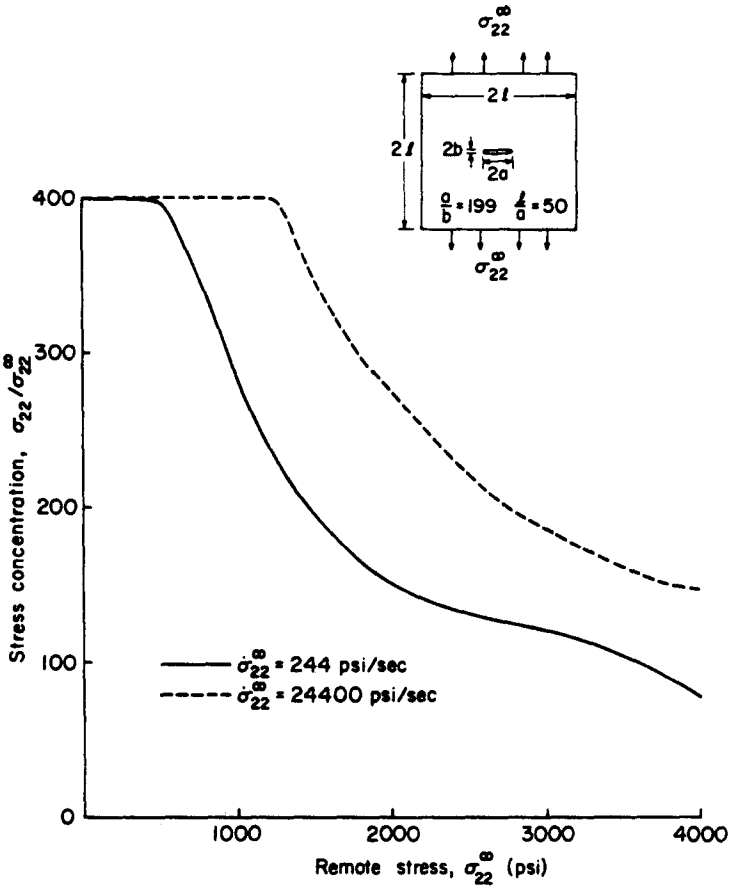

Fig. 5. Stress concentration at crack tip as function of time. Mode one. Power law creep model.

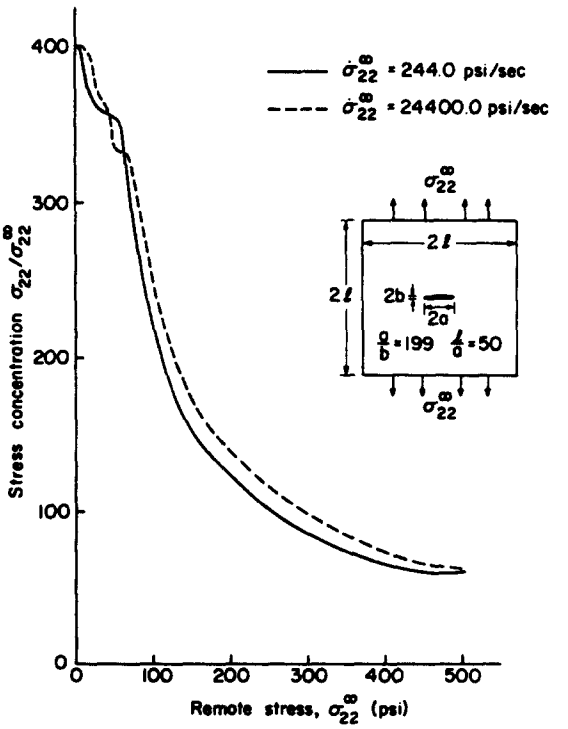

Fig. 6. Stress concentration at crack tip as function of time. Mode one. Hart's model.

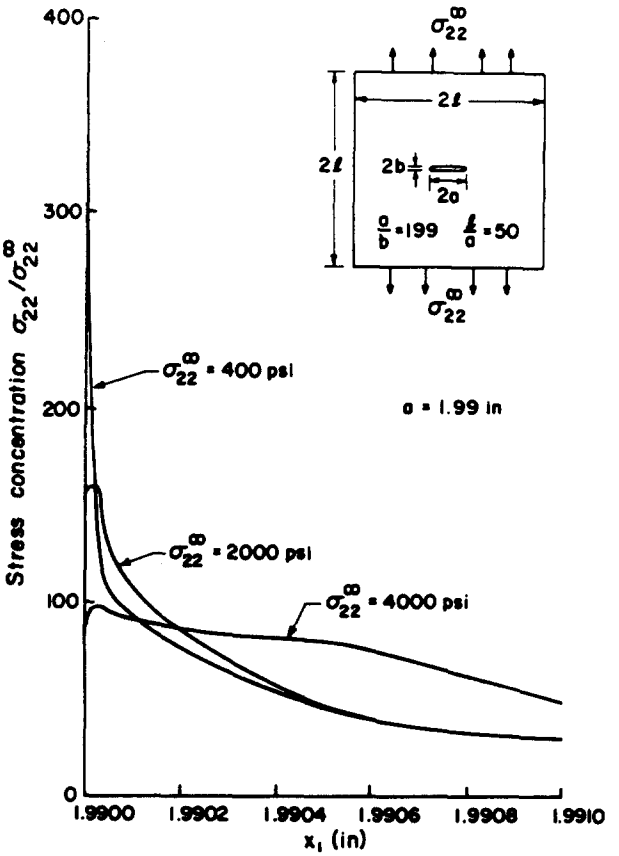

Fig. 7. Stress redistribution along the line $x_2 = 0$ in cracked plate. Mode one. Power law creep model. $\dot{\sigma}_{22}^{\infty} = 244$ psi/sec.

is the region where the stress invariant σ^a in the plastic element of Hart's model nearly equals the hardness and therefore causes substantial generation of permanent strain (i.e. large $\dot{\epsilon}^p$, see eqn (25)). This situation is analogous to yielding in classical plasticity.

Mode two crack results. The final example is that of the same cracked plate loaded remotely in shear with a constant stress rate $\dot{\sigma}_{12}^{\infty}$. In this case the elastic solution for an infinite plate gives zero stresses at the ends of both the major and minor axes of the ellipse and a stress concentration of $(a+b)^2/ab$ (about 201 in this case) at a point on the ellipse very near the crack tip. Forty boundary nodes are placed uniformly around the entire plate boundary. The stresses in this problem satisfy mirror symmetry (i.e. $\sigma_{ij}(x_1, x_2) = \sigma_{ij}(-x_1, -x_2)$) and because of this it is sufficient to distribute internal elements only in the upper half of the plate. The internal element distribution in the first quadrant is shown in Figs. 10(a) and (b) and a similar distribution is used in the second quadrant.

Results using Hart's model are shown in Figs. 11 and 12. The stress concentration is seen to decrease with time due to plastic flow and the viscoplastic region, starting at the point of stress concentration, is seen to move out in time.

The numerical results presented in this section are stable and the calculations with the power law creep model could be continued in time. For the Hart model, however, while the short time results reported here are stable, numerical problems are encountered if the calculations for cracked plates are continued into long times. A possible solution is the use of a simplified version of the constitutive model. Research on these lines is currently in progress.

Program statistics

The number of time steps and computer times required on an IBM 370/168, for these problems, are shown in Table 1. The elastic solution is seen to require the major portion of computer time. Once the elastic solution together with the proper matrices have been obtained, the time-dependent solution essentially requires multiplication of matrices and proceeds quite

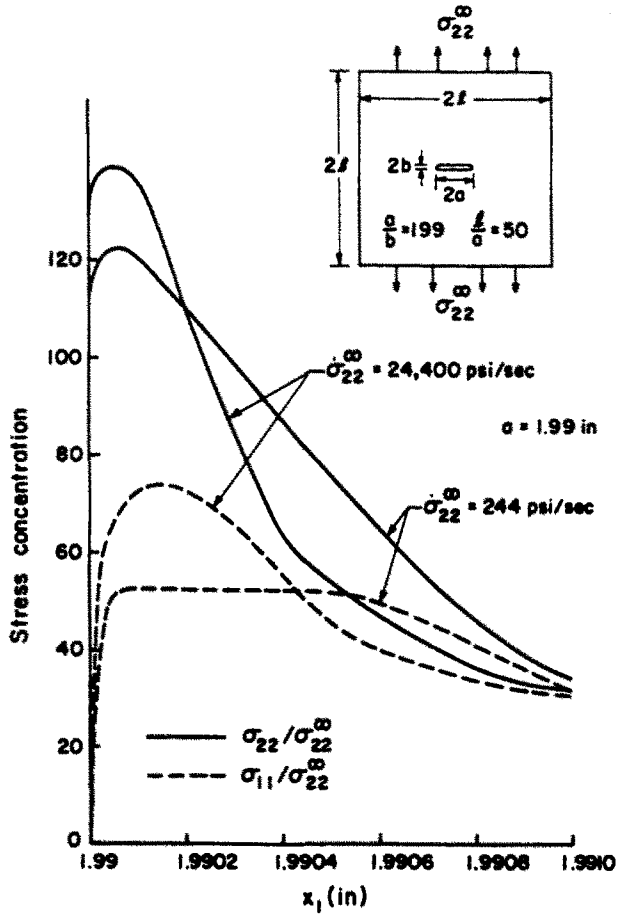

Fig. 8. Distribution of stresses along the line $x_2 = 0$ in cracked plate when $\dot{\sigma}_{22}^{\infty} = 222$ psi. Mode one. Hart's model.

rapidly. Of course, for a given geometry and loading, the elastic solution can be stored and reused. Thus, for example, the elastic solution for problems 2–5 in Table 1 is calculated only once.

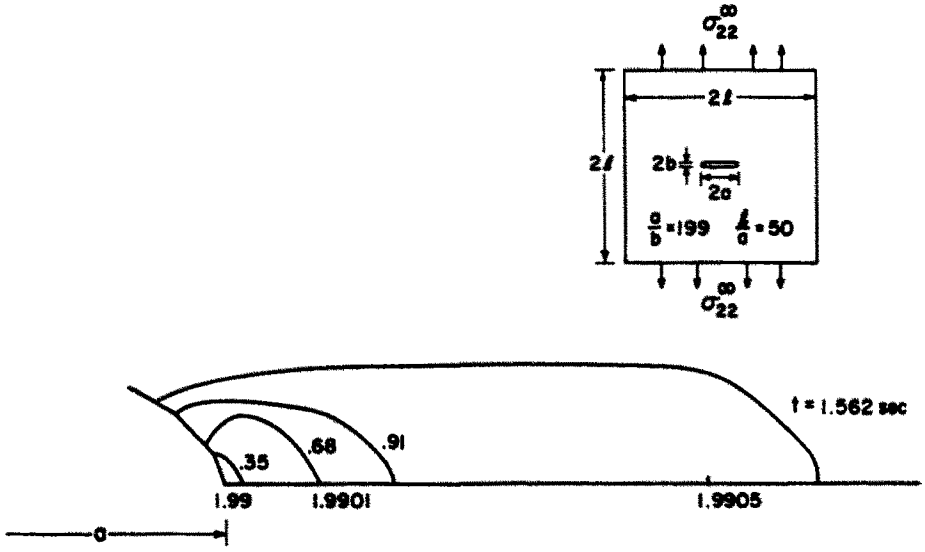

Fig. 9. Growth of viscoplastic region in cracked plate. Mode one. Hart's model. $\dot{\sigma}_{22}^{\infty} = 244$ psi/sec.

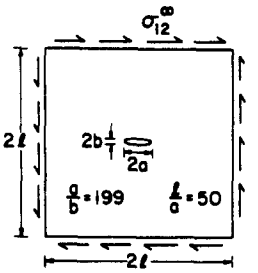

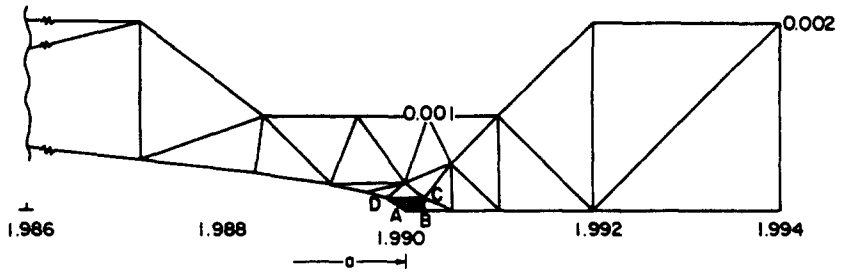

Fig. 10(a). Internal elements for cracked plate in shear.

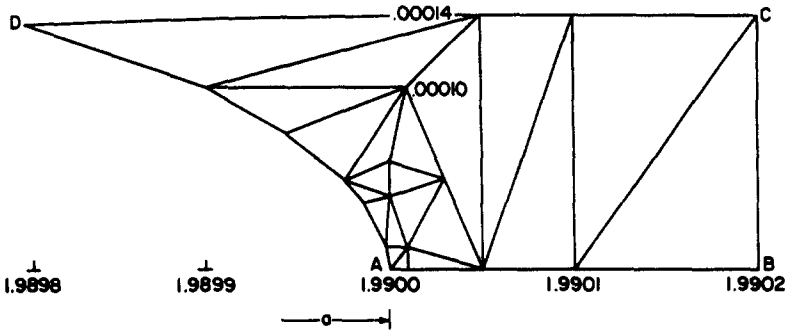

Fig. 10(b). Further details for Fig. 10(a).

CONCLUSIONS

A boundary element formulation for time-dependent inelastic deformation of plates with cutouts has been presented in a companion paper[1]. The formulation uses augmented kernels which guarantee that the cutout surface is traction free for all time. Since the effect of the cutout on the stress field is incorporated in the kernels, the cutout boundary need not be discretely modelled in a numerical solution scheme. Thus, this is an efficient and accurate method for calculation of stresses, especially near the crack.

Using this formulation, a numerical procedure for the determination of stresses in the near field of a stationary crack in a finite plate is presented here. A crack is modelled as a thin ellipse of axis ratio 199. The time-dependent redistribution of stresses near a tip of the major axis of the ellipse is calculated numerically for remote tensile (mode one) and shear (mode two) loading. The step-wise time integration of the rate equations proceeds rapidly and time-histories of the relevant variables is obtained within reasonable amounts of computer time. The constitutive models to describe material behavior, used in the numerical examples, are power law creep and the combined creep plasticity constitutive model of Hart. Other constitutive models having the same mathematical structure of the above can be easily incorporated into the formulation.

Table 1. Program statistics

Type of Problem	No. of Time Steps	C.P.U. (seconds) Elastic	Inelastic	Total
a/b = 4 Hart's law				
1. σ^{∞}_{22} = 4000 psi	462	137.4	31.9	169.3
a/b = 199 Power Law				
2. $\dot{\sigma}^{\infty}_{22}$ = 24400 psi/sec	900	158.6	45.3	203.9
3. $\dot{\sigma}^{\infty}_{22}$ = 244 psi/sec	2100	158.6	87.4	246.0
a/b = 199 Hart's Law				
4. $\dot{\sigma}^{\infty}_{22}$ = 24400 psi/sec	500	158.6	41.3	199.9
5. $\dot{\sigma}^{\infty}_{22}$ = 244 psi/sec	510	158.6	62.8	221.4
a/b = 199 Hart's Law				
6. $\dot{\sigma}^{\infty}_{12}$ = 244 psi/sec	600	393.1	176.5	569.6

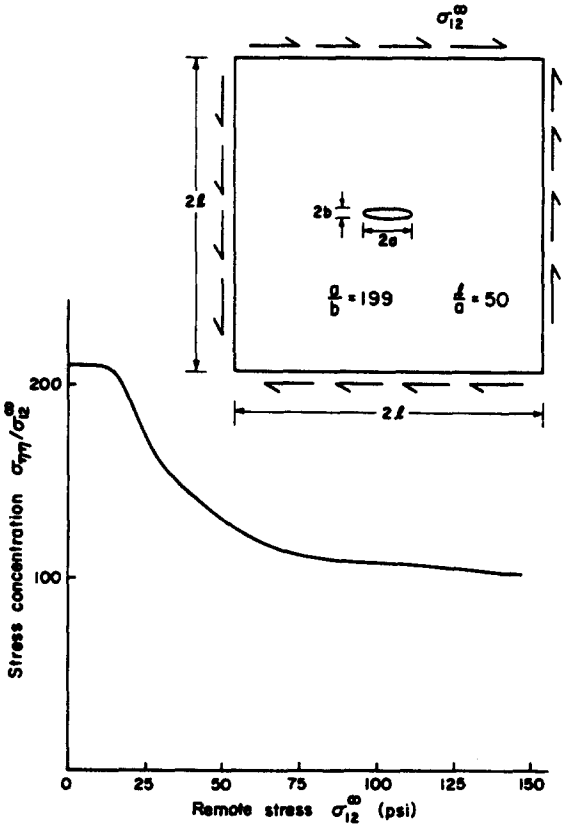

Fig. 11. Stress concentration on crack surface near the crack tip as function of time. Mode two. Hart's model $\dot{\sigma}^{\infty}_{12} = 244$ psi/sec.

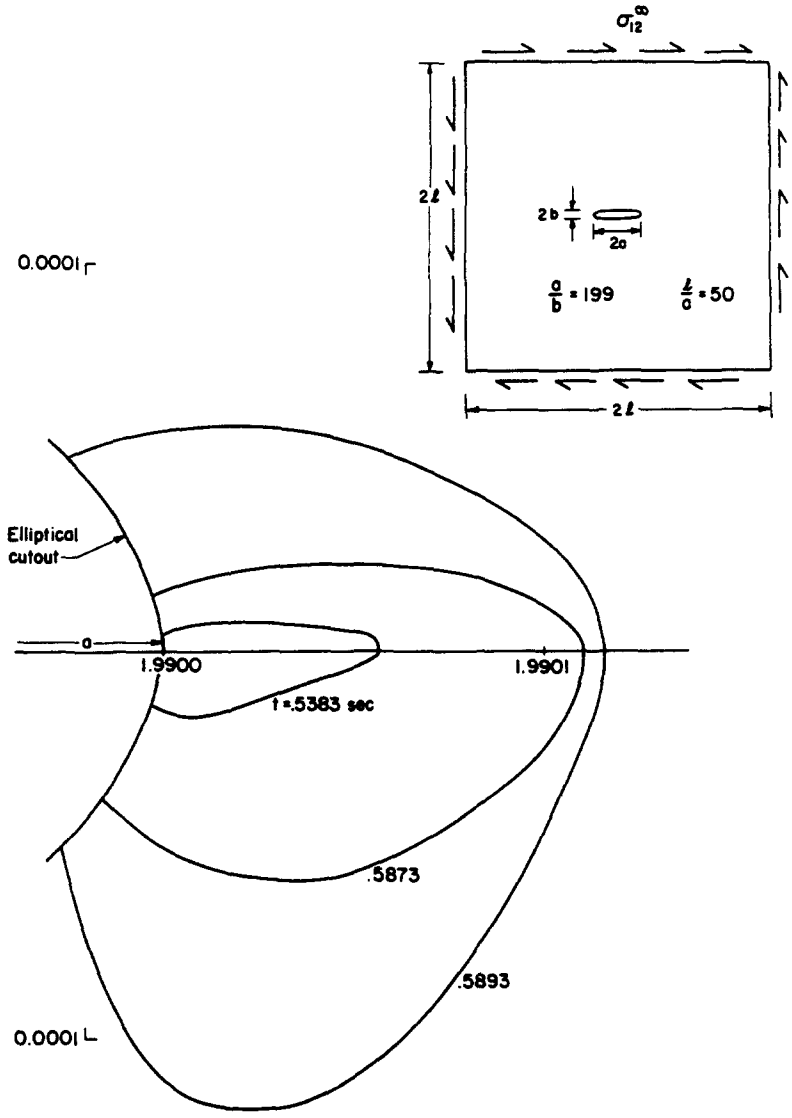

Fig. 12. Growth of viscoplastic region in cracked plate. Mode two. Hart's model. $\dot{\sigma}_{12}^{\infty} = 244$ psi/sec.

It is found that the stress concentration near the crack tip drops off quickly due to rapid plastic flow in this region. The stress relaxation is less at a rapid loading rate, compared to a slower loading rate, because there is less time for plastic flow in the former case. A viscoplastic region, starting at the point of stress concentration, is seen to move out in time.

Acknowledgement—This was supported by Contract No. EG-77-S-02-2733 of the U.S. Department of Energy with Cornell University.

REFERENCES

1. S. Mukherjee and M. Morjaria, A boundary element formulation for planar time-dependent inelastic deformation of plates with cutouts. *Int. J. Solids Structures* **17**, 115–126 (1981).
2. H. Riedel and J. R. Rice, Tensile cracks in creeping solids. *Presented at the ASTM Annual Symposium on Fracture Mechanics*, St. Louis (1979).
3. H. Riedel, Creep deformation at crack tips in elastic-viscoplastic solids. *Rep. No. MRL E-114*, Materials Research Laboratory, Brown University (1979).
4. M. Morjaria and S. Mukherjee, Improved boundary-integral equation method for time-dependent inelastic deformation in metals. *Int. J. Num. Meth. Engng* **15**, 97 (1980).
5. R. K. Penny and D. L. Marriott, *Design for Creep*. McGraw-Hill, London (1971).
6. E. W. Hart, C.-Y. Li, H. Yamada and G. L. Wire, Phenomenological theory—a guide to constitutive relations and fundamental deformation properties. In *Constitutive Equations in Plasticity* (Edited by A. S. Argon). MIT Press. Cambridge, Mass. (1976).

7. E. W. Hart, Constitutive relations for the nonelastic deformation of metals. *ASME J. Engng Mat. Tech.* **98**, 193 (1976).
8. N. I. Muskhelishvili, *Some Basic Problems of the Mathematical Theory of Elasticity* (trans. J. R. M. Radok). Noordhoff, Gronigen Holland (1953).
9. V. Kumar, M. Morjaria and S. Mukherjee, Numerical integration of some stiff constitutive models of inelastic deformation. *ASME J. Engng Mat. Tech.* **102**, 92 (1980).
10. V. Kumar, S. Mukherjee, F. H. Huang and C.-Y. Li, Deformation in Type 304 austenitic stainless steel, EPRI report EPRI NP-1276. Final Report for Project 697-1 by Cornell University (1979).
11. F. K. G. Odquist, *Mathematical Theory of Creep and Creep Rupture*. Clarendon Press, Oxford (1966).